Full length article

Effect of multi-domain structure on ionic transport, electrostatics, and current evolution in BaTiO₃ ferroelectric capacitor

CrossMark

Ye Cao [a,*], Jie Shen [b], Clive Randall [a], Long-Qing Chen [a]

[a] Department of Materials Science and Engineering, The Pennsylvania State University, University Park, PA 16802, USA
[b] Department of Mathematics, Purdue University, W Lafayette, IN 47907, USA

ARTICLE INFO

ABSTRACT

The semiconducting properties of certain ferroelectric materials, partially caused by the interactions among ferroelectric polarizations, charged domain walls, and conducting point defects, pose a threat to the reliability of ferroelectrics used as dielectric material in capacitor devices, and is not yet fully understood. We proposed a physical model combining the phase-field method for ferroelectric domain structures and diffusion equations for defect transport to study the resistance degradation behavior in multi-domain tetragonal BaTiO₃ capacitors. We considered a hypothetical Ni/BaTiO₃/Ni single parallel plate capacitor configuration subject to 0.5 V dc bias at 25 °C. It is found that 90° domain walls are charged, induce local space charge segregation, and form local electric potential barriers upon external bias that significantly influence the ionic transport behavior. Additionally, the 180° domain walls remain nearly charge neutral and have much less influence on ionic transport. The effect of domain wall and polarization orientations on the leakage current evolution is investigated. Our study could necessitate further understanding on the influence of ferroelectric state, ionic interactions, transport barriers, spatial distributions, and breakdown phenomena.

© 2016 Acta Materialia Inc. Published by Elsevier Ltd. All rights reserved.

1. Introduction

Ferroelectric oxides, such as barium titanite (BaTiO₃), have been extensively used as dielectric materials in multi-layer ceramic capacitors (MLCCs) in various electronic devices [1]. The trend of further miniaturization of MLCC devices for high capacitance resulted in ever-decreasing dielectric thickness, down to submicron levels, and ever-increasing electric field strength distributed across each dielectric layer under given voltage stresses [2]. This causes a major challenge to the reliability of MLCCs, among which the long-term resistance degradation is one of the primary limiting factors to the life time of MLCCs. The long-term resistance degradation is characterized by slowly increasing leakage currents under a DC bias well below the critical breakdown voltage [3].

In the dielectric industry, the evaluations of resistance degradation, and thus the long-term reliability of MLCCs, are generally accessed by an engineering approach called the highly accelerated lifetime tests (HALTs) [3,4]. This method evaluates the lifetime of MLCCs by extrapolating the HALTs data measured under various temperatures and field stresses to the real working condition based on the Erying model [5]. Although this method shows advantages in accelerating the measurement at high temperature and voltage stress in paraelectric phase, it rules out the possible influence of complex ferroelectric domain structures and the associated piezoelectric strains on the degradation process of ferroelectric-based capacitor. Therefore, the HALTs evaluated long-term reliability accessed in the paraelectric phase may not represent the real lifetime of ferroelectric capacitors.

On the other hand, it is of scientific importance to understand the mechanism of the ion transport and its relationship to resistance degradation. Over the past 20 years, it has been investigated by a number of experimental approaches, including the electro-coloration measurement [6,7], impedance spectroscopy (IS) [8], thermal simulated depolarization current (TSDC) [9,10], transmission electron microscopy (TEM) [11], and theoretical calculations, such as finite element method [12–14]. While it is generally recognized that the oxygen vacancy migration plays an important role in the degradation process, it is still unclear how the ferroelectric domain structures could influence the ionic/electronic distribution and transport behavior. The authors have recently studied the effect of ferroelectric polarization on resistance

---

* Corresponding author.
  E-mail address: yxc238@psu.edu (Y. Cao).

degradation behavior in single domain BaTiO$_3$ capacitor [15]; however, a single domain configuration is rarely formed in real BaTiO$_3$ capacitors. It was reported that domain walls contribute to the dielectric and piezoelectric properties of ferroelectric materials [16,17] and could pin the local space charge and affect the transport behavior due to the polarization charges [18–21] and mechanical stresses [22,23] developed along ferroelastic domain walls. Therefore, to obtain a more complete fundamental understanding of resistance degradation behavior in ferroelectric capacitor, a physics-based theoretical model capable of incorporating the multi-domain structure and defect transport interaction is imperative.

In this work, we developed a combined phase-field and transport model to understand the role of ferroelectric domain and domain walls on ionic transport and resistance degradation behavior, and to estimate the long-term reliability of real ferroelectric based capacitor. The phase-field method has been successfully applied to studying the ferroelectric domain structures in both bulk and thin film systems [24–28]. In this study, we chose the sandwiched Ni/BaTiO$_3$/Ni single parallel plate capacitor configuration as the model system. The effects of ferroelectric/metal interfaces and domain wall orientations on the ionic segregation/depletion, local electric potential and field distribution, and ionic migration upon external field and leakage current evolution have been extensively studied. Our work provides some fundamental insights into the complex interactions among ferroelectric domain structure, defect transport and dielectric degradation behavior.

2. Model

In the phase-field model of multi-domain BaTiO$_3$ capacitor, the ferroelectric system is represented by choosing the polarization vector $P_i = (P_1, P_2, P_3)$ as the order parameter to describe the ferroelectric domain structures. The domain evolution is modeled by the temporal evolution of P_i obtained by minimizing the total free energy of the system with respect to P_i,

$$\frac{\partial P_i(\mathbf{r}, t)}{\partial t} = -L \frac{\delta F}{\delta P_i(\mathbf{r}, t)}, (i = 1 \sim 3) \tag{1}$$

in which t is the time step and L is the kinetic coefficient related to domain mobility. The total free energy F of BaTiO$_3$ single crystal is expressed as,

$$F = \int_V \left[f_{\text{lan}}(P_i) + f_{\text{grad}}(P_{i,j}) + f_{\text{elas}}(P_i, \varepsilon_{ij}) + f_{\text{elec}}(P_i, E_i) \right] dV \tag{2}$$

where V is the system volume, ε_{ij} and E_i denote the components of strain and electric field, $P_{i,j} = \partial P_i / x_j$, and $f_{\text{lan}}(P_i)$, $f_{\text{grad}}(P_{i,j})$, $f_{\text{elas}}(P_i, \varepsilon_{ij})$ and $f_{\text{elec}}(P_i, E_i)$ represent the Landau-Devonshire free energy density, the gradient energy density, and elastic energy density and the electrostatic energy density, respectively. Detailed expressions of each of the local free energy densities can be found in literature [25,26].

The charge defect distribution, transport, and blocking at electrodes play an important role in resistance degradation phenomena. In this study, the intrinsic and extrinsic major charge defects of interest include the oxygen vacancies ($V_O^{\cdot\cdot}$), electrons ($e^{'}$), holes ($h^{\bullet}$), and ionized acceptors ($A^{'}$) written in Kröger-Vink notation [29]. The +2 oxygen vacancies are created during high temperature annealing of capacitors, and their concentration is assumed to be conserved at the temperature when degradation measurements are conducted. The acceptors are introduced by substitution of +3 elements, such as Fe and Al, on the +4 Ti sites ($Fe_{Ti}^{'}$ and $Al_{Ti}^{'} = A^{'}$) and

are considered fully ionized and immobile.

We assumed in the simulation that all the charged carriers are homogeneously distributed in the entire BaTiO$_3$ layer, and local charge neutrality condition is satisfied in the initial state,

$$\rho(x) = \sum_i z_i e_0 c_i(x) = 0 \quad (i = V_O^{\cdot\cdot}, p, n, A^{'}) \tag{3}$$

where $\rho(x)$ is the space charges at position x, e_0 is the unite charge, c_i and z_i are the concentration and charge number of given species i. ($z_{V_O^{\cdot\cdot}} = +2, z_{h^{\cdot}} = +1$ and $z_{e^{'}} = z_{A^{'}} = -1$) The migrations of the mobile charge defects are described by solving the linear transport equations, considering only concentration gradient and local electric field as the driving forces,

$$\vec{J}_i = -D_i \vec{\nabla} c_i + z_i \mu_i c_i \vec{E} \frac{\partial c_i}{\partial t} = -\vec{\nabla} \cdot \vec{J}_i \tag{4}$$

in which J_i, D_i, μ_i denote the flux, diffusivity, and mobility of given charge species i. $\vec{\nabla} = \frac{\partial}{\partial x} \vec{i} + \frac{\partial}{\partial y} \vec{j} + \frac{\partial}{\partial z} \vec{k}$ is the gradient operator. $\vec{E}$ is the local electric field component. We assume that the plate electrodes form blocking contact to the oxygen vacancy transport, thus the boundary condition of Eq. (4) for oxygen vacancy is specified as,

$$\vec{J}_{V_O^{\cdot\cdot}} = 0 \tag{5}$$

On the other hand, the mobility of electrons and holes are several orders of magnitude higher than that of oxygen vacancy. They are assumed to reach steady state for each oxygen vacancy evolution. Mathematically we solve the steady state equations for electron ($\partial n / \partial t = 0$) and hole evolution ($\partial p / \partial t = 0$). The electronic concentrations at the metal/ferroelectric interfaces are fixed by the work function of the metal electrode (Ni). The boundary conditions of Eq. (4) for electrons and holes are written as,

$$n_{z=0.L} = N_c \exp\left(-\frac{E_c - E_{fm}}{k_B T} \right)$$
$$p_{z=0.L} = N_v \exp\left(-\frac{E_{fm} - E_v}{k_B T} \right) \tag{6}$$

in which N_c and N_v are the effective density of states in the conduction and valence band of BaTiO$_3$, where E_c and E_v represent the energy of the conduction band minimum and valence band maximum. E_{fm} is the work function of plate electrode, and k_B is the Boltzmann constant.

The interaction between electric potential, space charge, and polarization induced bound charge are described by the electrostatic equilibrium equation considering the space charge distribution,

$$D_{i,i} = D_{1,1} + D_{2,2} + D_{3,3} = \rho \tag{7}$$

in which $D_{i,i} = \partial D_i / \partial x_i$ while D_i is the electric displacement, which is related to the electric field and polarization component through,

$$D_i = \kappa_0 \kappa_{ij} E_j + P_i (i = 1 \sim 3) \tag{8}$$

in which κ_0 is the vacuum permittivity and κ_{ij} is the dielectric constant. The polarization induced charges are introduced by $-P_{i,i} = -(P_{1,1} + P_{2,2} + P_{3,3})$, and the electric field $\vec{E}$ is related to the electric potential through,

$$E_i = -\phi_{,i} (i = 1 \sim 3) \tag{9}$$

Combining Eqs. (7)–(9) and assuming $\kappa_{ij} = 0 (i \neq j)$, the
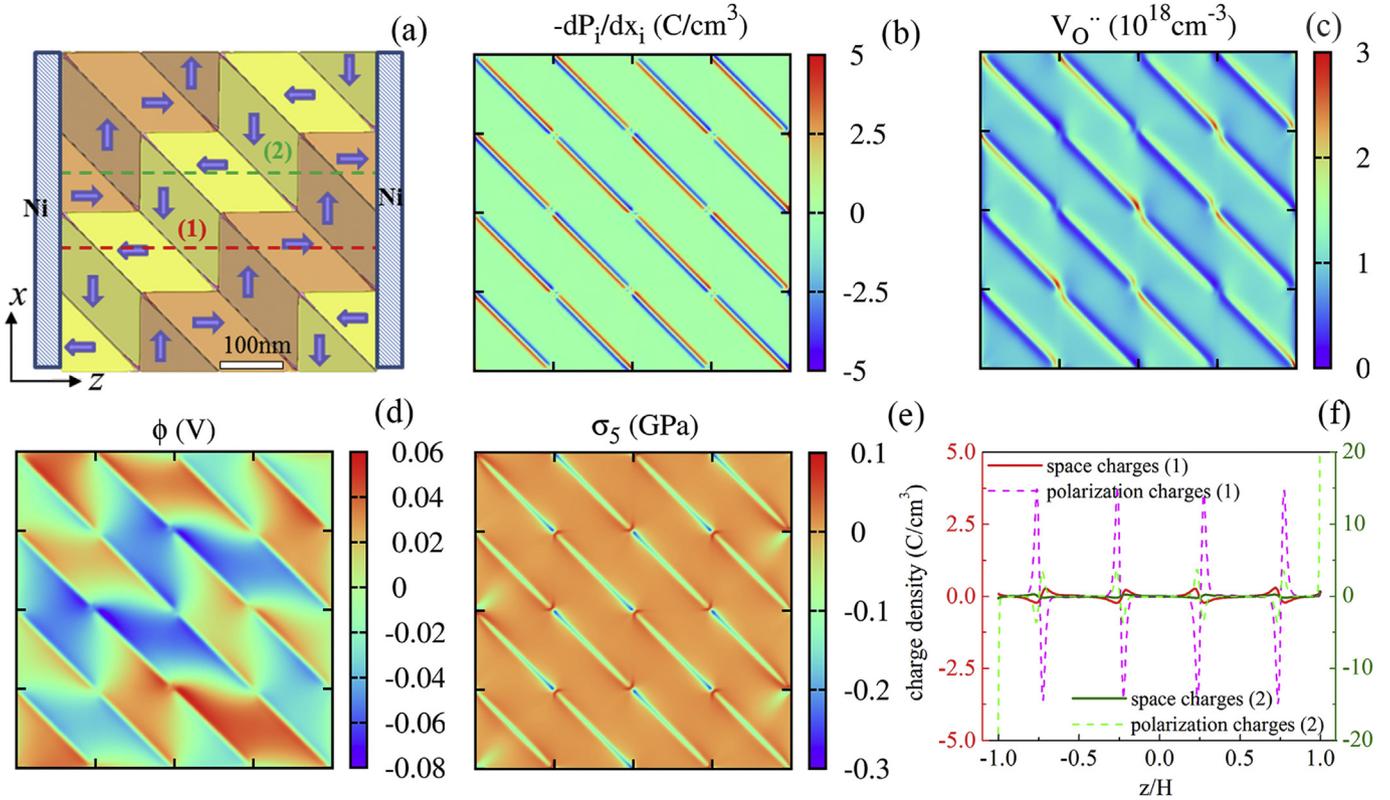
Fig. 1. 2D plot of the equilibrium state of (a) domain structure, (b) polarization induced bound charges ($i = 1-3$), (c) oxygen vacancy distribution, (d) electric potential distribution and (e) shear stress σ_5. (f) 1D comparison of space charge (solid lines) and polarization charge (dashed lines) distributions along particular directions as indicated by the red and green dashed lines in (a). The red and green ordinates in (f) (note with different scales) are for charge distributions along direction (1) and (2) respectively as indicated in (a). (For interpretation of the references to colour in this figure legend, the reader is referred to the web version of this article.)

electrostatic equilibrium equation (Eq. (7)) can be rewritten as,

$$\kappa_{11}\phi_{,11} + \kappa_{22}\phi_{,22} + \kappa_{33}\phi_{,33} = \frac{1}{\kappa_0}\left(P_{1,1} + P_{2,2} + P_{3,3} - \rho\right) \quad (10)$$

The boundary condition for Eq. (10) is defined as,

$$\phi|_{z=0} = V_a(0), \quad \phi|_{z=L} = V_a(L) \quad (11)$$

in which $V_a(0)$ and $V_a(L)$ are specified from the externally applied potential bias at $z = 0, L$.

To model the polarization induced bound charges at the Ni/BaTiO₃ interfaces, we specify the polarization distribution at the boundaries as,

$$a \times P_i - b \times \left.\frac{dP_i}{dz}\right|_{z=0} = 0, \quad a \times P_i + b \times \left.\frac{dP_i}{dz}\right|_{z=L} = 0 (i = 1 \sim 3) \quad (12)$$

where the coefficients a and b are chosen to be 1.0 and 0.05 cm to represent the case where the charges at the metal/ferroelectric interfaces are partially compensated.

The current density is contributed from the flow of mobile charged defects, including oxygen vacancies, electrons, and holes. The current density for particular charged carrier i and the total current density are given by,

$$\begin{aligned} I_i &= z_i e_0 J_i \\ I_{total} &= \sum_i I_i \end{aligned} \quad (13)$$

where i only include mobile species ($i = V_O^{\cdot\cdot}, e', h^{\cdot}$).

3. Simulation results and discussion

3.1. Initial setup

We started with a preset 2D multi-domain tetragonal BaTiO₃ as the model system, which consists of four possible domain variants, i.e., $a+(100)$, $a-(-100)$, $c+(001)$, and $c-(00-1)$ in a head-to-tail configuration to form both 180° and 90° domain walls (Fig. 1(a)). The BaTiO₃ film is 500 nm in thickness and is constrained by Ni plate electrodes of normal vector along z (001). The external applied bias is along $+z$ direction. We set up a coordinate system

Table 1
Parameters used in the simulation.

Parameter	Value	Parameter	Value
Temperature, T (K)	298	Conduction band, E_c (eV) [19]	−3.6
Total thickness, L (nm)	500	Valence band, E_v (eV)	−6.7
External applied bias (V)	0.5	Work function of Ni electrode, E_{fm} (eV)	−5.2
Oxygen vacancy mobility, $\mu_{V_O^{\cdot\cdot}}$ (cm²·V⁻¹·s⁻¹) [7]	1.0×10^{-14}	Effective Density of States, N_c, N_v (cm⁻³) [12]	10^{22}
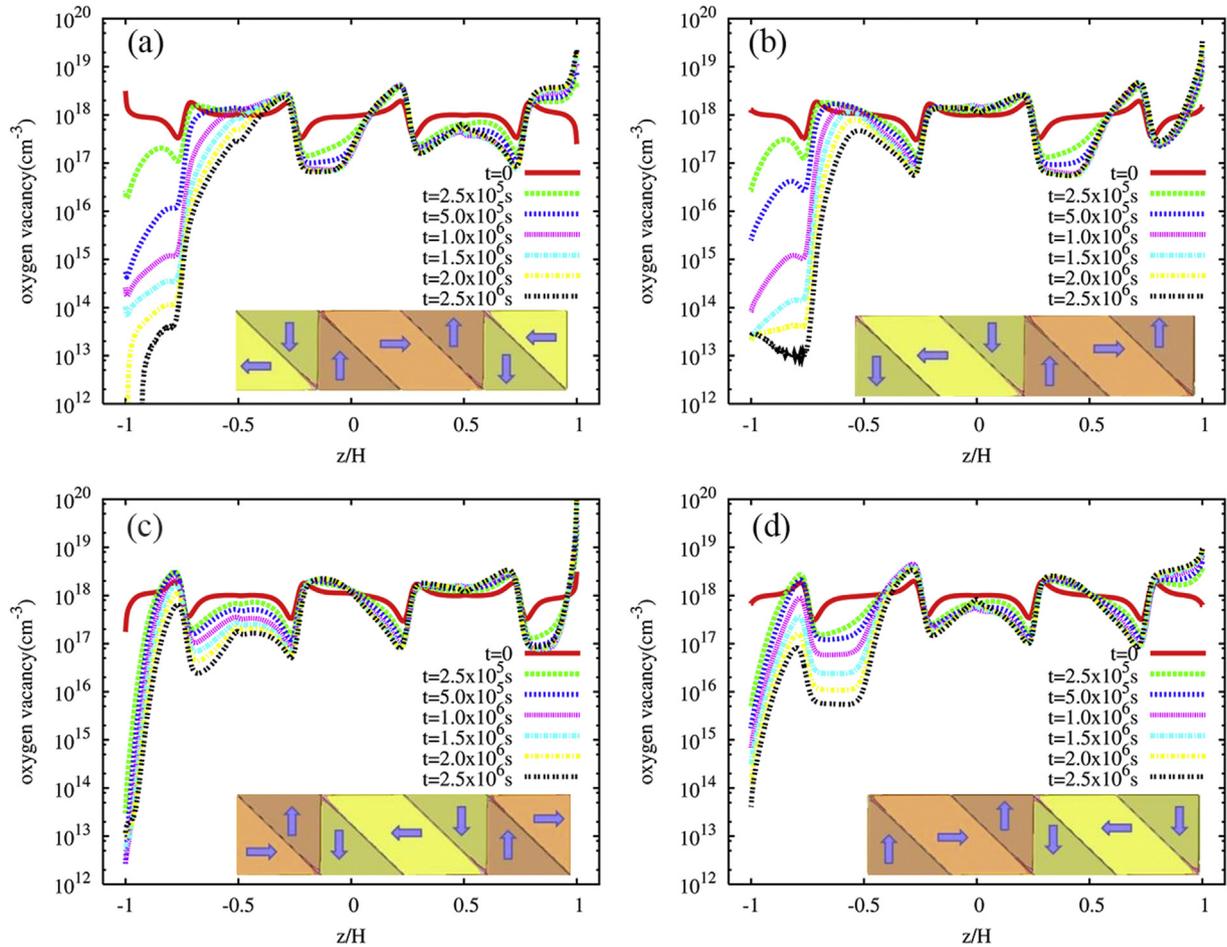
Fig. 2. 1D plot of oxygen vacancy evolution along z direction in each of the 1/4 of the entire multi-domain BaTiO$_3$ under U$_{DC}$ = 0.5 V at room temperature: (a) x/H = 0.0–0.5; (b) x/H = 0.5–1.0; (c) x/H = 1.0–1.5; (d) x/H = 1.5–2.0. (H = 250 nm is half of the film thickness, so that z/H from −1 to +1 represents the entire film thickness).

with periodic boundary condition along x (100) direction and non-periodic general boundary condition along z (001) direction. The simulation size is discretized into a 2D mesh of 400Δx × 400Δz, while Δz is non-uniform. The temporal evolution of the polarizations and defect concentrations are obtained by solving the time-dependent Ginzburg-Laudau (TDGL) equations (Eqs (1)) and transport equations (Eqs (4)) using the combined semi-implicit Fourier spectral method [30] and Chebyshev collocation method [31]. The material constants and energy coefficients are taken from the literature [28]. The parameters used in the simulation are listed in Table 1.

3.2. Equilibrium state

We first evolved the preset domain structure under room temperature without an external bias (U$_{DC}$ = 0) to reach equilibrium state, in which both 90° and 180° domain walls become stable and form a step-like domain configuration (Fig. 1(a)). It is clearly seen that the positive/negative alternating polarization charges are bounded to the 90° domain walls, while the 180° domain walls and the domain interior remain charge neutral (Fig. 1(b)). This is due to the gradual rotations of polarizations across 90° domain walls of finite thickness. The 90° charged domain walls are locally compensated by an ionic (oxygen vacancy) segregation (Fig. 1(c)). It should be noted that the electronic charge compensation is negligible, since electronic charges are assumed to be fixed at the metal/ferroelectric interfaces in the simulation, and consequently their

concentrations are much lower than ionic charge carriers. The ionic charges do not fully compensate the polarization bound charges. This induces a small internal electric potential even in the absence of external applied bias (Fig. 1(d)), and a negative shear stress (σ$_5$) along the 90° domain walls (Fig 1(e)). A 1-D plot of the charge distributions along particular directions (indicated by red and green dashed lines in (a)) clearly shows that only 90° domain walls exhibit alternating polarization charges (dashed lines in (f)) and space charges (solid lines in (f)) (always in the opposite direction for compensation), with the latter being much smaller than the former in magnitude. The resulting net charges are between −5.0–5.0 C/cm^3 across the 90° domain walls. Notably large polarization charges are also found at the metal/ferroelectric interfaces, where the polarizations are oriented perpendicular to the contacting plate electrodes (green dashed lines in (f), not shown in (b)). This is because the electrodes are assumed to partially compensate the polarization charges. When the polarizations are oriented parallel to the contacting electrodes, there are no interfacial charges induced (pink dashed lines in (f)).

3.3. Evolution under applied bias

When the domain structure and the local charges reach an equilibrium state, a dc bias of 0.5 V is applied along + z direction. Fig. 2(a)–(d) show the temporal evolution of oxygen vacancies along z directions across the center of each of the 1/4 sections of the entire domain (the corresponding domain structures are shown in
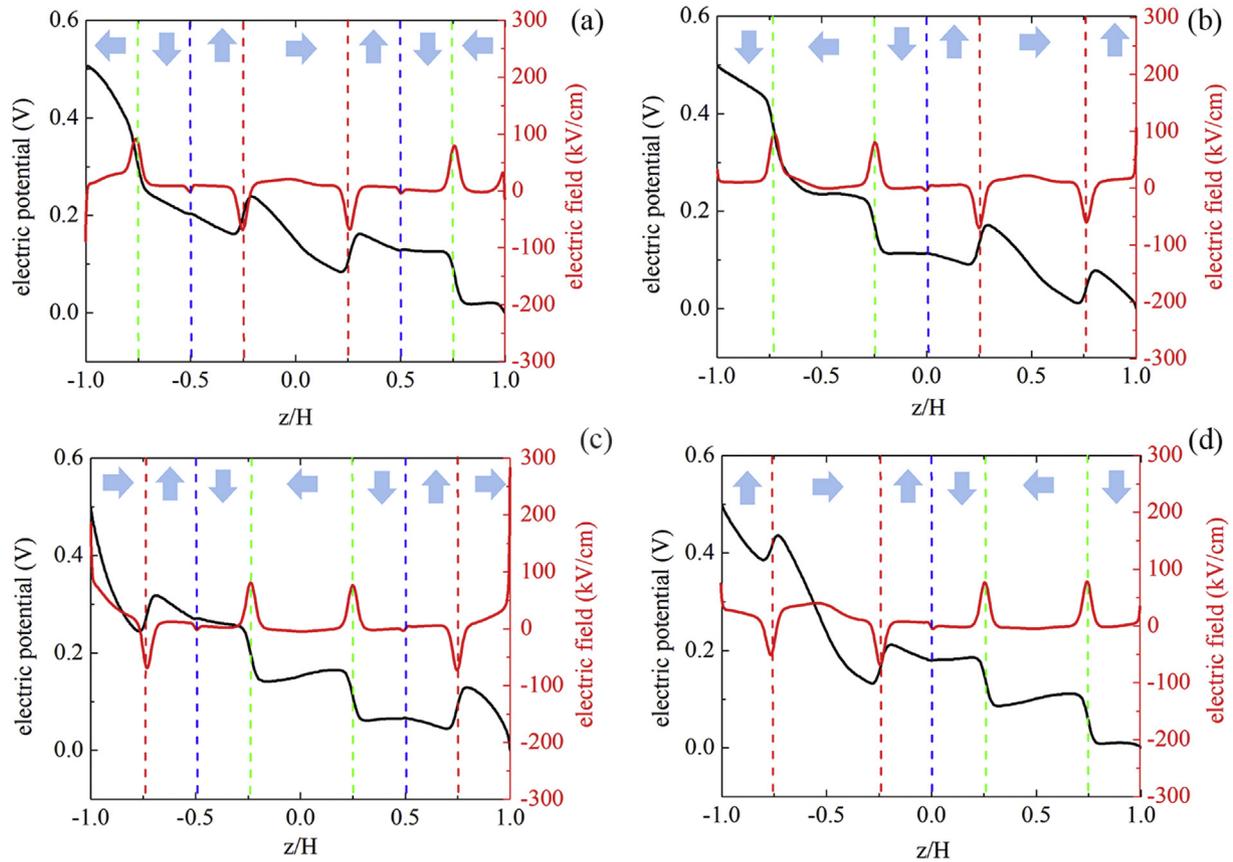
Fig. 3. 1D plot of electric potential (black solid lines) and electric field (red solid lines) distributions at t = 2.5 × 10^6s along z direction in each of the 1/4 of the entire multi-domain BaTiO$_3$ under U$_{DC}$ = 0.5 V at room temperature: (a) x/H = 0.0–0.5; (b) x/H = 0.5–1.0; (c) x/H = 1.0–1.5; (d) x/H = 1.5–2.0. The light blue arrows indicate the domain orientations. Dark blue dashed lines indicate the positions of 180° domain walls, green dashed lines indicate the positions of 90° domain walls (↓\←\↓) where electric potential locally drops, and red dashed lines indicate the positions of 90° domain walls (↑\→\↑) where there is local electric potential barrier blocking the ionic transport. (For interpretation of the references to colour in this figure legend, the reader is referred to the web version of this article.)

the insets). Under the applied bias, oxygen vacancies electromigrate towards the cathode side (z/H = 1.0), which results in ionic segregation in the vicinity of the cathode region and depletion in the anode region (z/H = −1.0). It is also seen that part of the oxygen vacancies pile up in front of the 90° domain walls and under these conditions are locally trapped and not free to migrate towards cathode, due to the polarization charges along 90° domain walls. This becomes obvious in those domains with local polarizations oriented along the transport direction (+z), where ionic enrichment and depletion are both seen locally inside the domain. Such local ionic redistribution are also seen in domains of polarization orientation opposite to the transport direction (−z), but the extent of local enrichment/depletion is less than the previous case. On the other hand, 180° domain walls are less, if not at all, charged and have nearly no influence on the oxygen vacancy transport. Clearly, the polarizations along + z directions tend to promote the oxygen vacancy transport, as is further evidenced by the maximum local oxygen vacancy accumulation of ~10^{20} cm^{-3} found at the cathode region, where adjacent domain is along + z (Fig. 2(c)) and agrees with previous report [15].

To further understand the interaction between the 90° domain walls and ionic transport, we studied the electric potential and field distribution under U$_{DC}$ = 0.5 V. Fig. 3(a)–(d) show the 1D electric potential (solid black lines) and electric field (solid red lines) distributions across the center of each of the 1/4 sections of the entire domain at time t = 2.5 × 10^6s. The light blue arrows represent the domain orientations along z directions, while the dashed lines

indicate the domain wall positions. From Fig. 3, the electric potential drops are mainly seen in "→" oriented domains along the applied field direction. This also explains why oxygen vacancy transports are promoted in those local domains (Fig. 2). The electric potential drops become much smaller in domains with "←", "↓" and "↑"orientations that are not adjacent to the electrodes. On the other hand, remarkable electric potential gradients and local electric field enhancements can be found across the 90° domain walls (indicated by red and green dashed lines). For "↓\←" and "←\↓" types of domain walls (indicated by green dashed lines), the drops of electric potential induce local positive electric fields of ~+100 kV/ cm. The oxygen vacancy drift under this positive field counterbalances oxygen vacancy diffusion in the opposite direction due to the local concentration gradient, which is induced by the polarization charges located at the 90° domain wall. This is further illustrated by a combined replot of Figs. 1(f), 2(b) and 3(b) into Fig. 4. For "↑\→" and "→\↑" types of domain walls (indicated by red dashed lines), local potential barriers are formed with negative local electric fields to block the ionic transport. This causes local ionic accumulation and depletion on each side of the 90° domain walls. The 180° domain walls (indicated by blue dashed lines in Fig. 3) are less interacted with the electric potential distributions, and the electric fields are much smaller than those found at 90° domain walls.

3.4. Influence of domain structure on leakage current evolutions

The effects of multi-domain structures on leakage current
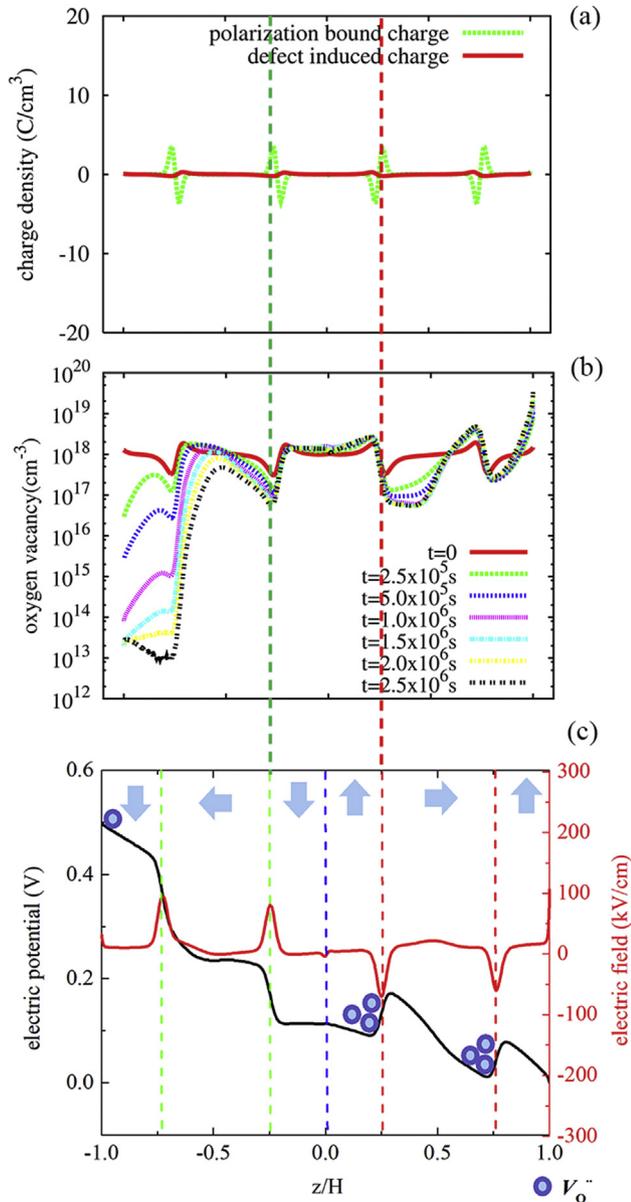
Fig. 4. Illustration of interactions between polarization charges, ionic transport, and electric potential/field by replotting Figs. 1(f), 2(b) and 3(b) into Fig. 4(a)–(c). The electric potential drop at the 90° domain wall (green dashed lines) induces local positive electric field to facilitate the oxygen vacancy drift (c), and counterbalances the oxygen vacancy diffusion in the opposite direction due to local concentration gradient (b), which is induced by the positive/negative polarization charges aside the 90° domain wall (a). (For interpretation of the references to colour in this figure legend, the reader is referred to the web version of this article.)

Fig. 5. (a) Schematic plot of possible domain configurations of BaTiO$_3$ and (b) comparison of current density evolution of BaTiO$_3$ capacitor of different domain configurations at 25 °C under U_{DC} = 0.5 V. The colors of the schematic domain configurations in (a) correspond to the colors of the current density evolution in (b). The "+" mark the degradation characteristic time (t_{ch}) for different domain configurations. (For interpretation of the references to colour in this figure legend, the reader is referred to the web version of this article.)

evolution in Ni/BaTiO$_3$/Ni single layer capacitor under DC bias are further investigated. For comparison, we considered four additional scenarios of BaTiO$_3$ composed of: (1) single domain of P$_z$ along + z direction (along the applied field direction), (2) single domain of P$_z$ along -z direction, (3) 90° domain structure composed of "↑\→" and "→\↑" types of domain walls, and (4) 90° domain structure composed of "↓\←" and "←\↓" types of domain walls. They are schematically illustrated in Fig. 5(a), and the current density evolutions for scenario (1)−(4) and multi-domain structure (5) are plotted and compared in Fig. 5(b). It is seen that the leakage currents increase slowly in the initial steps, followed by a fast and significant increase, which indicates the dielectric breakdown of capacitors. The sudden increases of leakage currents are attributed

to the oxygen vacancy migrations and accumulations at the cathode regions. By comparing the degradation characteristic time (t_{ch}), which is defined as the critical time when leakage current increases 10 × compared to its initial value (marked by "+" in Fig 5(b)), it is found that t_{ch} is fastest in single c+ domain (t_{ch} ~ 4.6 × 10^{5}s, scenario (1)) and slowest in single c-domain (t_{ch} > 2 × 10^{6}s, scenario (2)). Clearly, the polarization accelerates the degradation process when it is in the field direction (+z). Similarly the leakage currents in "↑\→\↑" type of 90° domain structure (t_{ch} ~ 7.7 × 10^{5}s, scenario (3)) increase faster than in "↓\←\↓" type of 90° domain structure (t_{ch}~1.28 × 10^{6}s, scenario (4)). This is because the trend of the polarization direction is still along the applied field direction in (3) and reverses to the field direction in (4). Notably, t_{ch} in (3) is also slower than that in (1), since domain structure of (3) consists of half a+ and c+ domain types, with only c+ contributing to the current evolution and the rest a+ less interacted with the ionic transport. The charged 90° domain walls in (3) could also impede the oxygen vacancy migration and, consequently, the leakage current increase. Conversely, the current increases faster in (4) compared to (2), since the former structure consists of only half c-domain that is known to inhibit current increase. Finally, the multi-domain structure is considered a combination of all possible a/c domains and 180°/90° domain walls; therefore, the t_{ch} is expected to be average of the other four scenarios (t_{ch} ~ 9.4 × 10^5 s).

4. Conclusions

In this work, we developed a phase-field model combined with transport equations to study the space charge distribution, ionic transport, electrostatic evolution, and resistance degradation of a preset multi-domain structure BaTiO$_3$ single plate ferroelectric capacitor. Our results show that polarization induced bound charges along 90° domain walls account for the local oxygen vacancy segregation, while the 180° domain walls and domain interiors remain charge neutral and have less influence on the defect distribution. Upon an external DC bias, remarkable electric

potential gradient and potential barrier, and the resulting local electric field concentration, are observable at the 90° charged domain walls, which partially blocks the oxygen vacancies migration, resulting in a local ionic enrichment and depletion on either side of the 90° domain walls. On the other hand, the effect of 180° domain walls on local electrostatics and oxygen vacancy evolution is hardly seen. The influence of multi-domain structure on the resistance degradation behavior under room temperature is further investigated by comparing the leakage current evolutions and degradation characteristic time (t_{ch}) among different possible domain configurations in $BaTiO_3$.

Acknowledgements

References

[1] H. Kishi, Y. Mizuno, H. Chazono, Base-metal electrode-multilayer ceramic capacitors: past, present and future perspectives, Jpn. J. Appl. Phys. 1 (42) (2003) 1–15.

[2] A.V. Polotai, A.V. Ragulya, C.A. Randall, Preparation and size effect in pure nanocrystalline barium titanate ceramics, Ferroelectrics 288 (2003) 93–102.

[3] R. Waser, T. Baiatu, K.H. Hardtl, Dc electrical degradation of perovskite-type titanates .1. Ceramics, J. Am. Ceram. Soc. 73 (1990) 1645–1653.

[4] S. Zhao, S.J. Zhang, W. Liu, N.J. Donnelly, Z. Xu, C.A. Randall, Time dependent dc resistance degradation in lead-based perovskites: 0.7 Pb($Mg_{1/3}Nb_{2/3}$)O_3-0.3 $PbTiO_3$, J. Appl. Phys. 105 (2009) 053705.

[5] C.A. Randall, R. Maier, W. Qu, K. Kobayashi, K. Morita, Y. Mizuno, N. Inoue, T. Oguni, Improved reliability predictions in high permittivity dielectric oxide capacitors under high dc electric fields with oxygen vacancy induced electromigration, J. Appl. Phys. 113 (2013) 014101.

[6] R. Waser, T. Baiatu, K.H. Hardtl, Dc electrical degradation of perovskite-type titanates .2. Single-Crystals, J. Am. Ceram. Soc. 73 (1990) 1654–1662.

[7] H.I. Yoo, M.W. Chang, T.S. Oh, C.E. Lee, K.D. Becker, Electrocoloration and oxygen vacancy mobility of $BaTiO_3$, J. Appl. Phys. 102 (2007) 093701.

[8] W. Liu, G.Y. Yang, C.A. Randall, Evidence for increased polaron conduction near the cathodic interface in the final stages of electrical degradation in $SrTiO_3$ crystals, Jpn. J. Appl. Phys. 48 (2009) 051404.

[9] W. Liu, C.A. Randall, Thermally stimulated relaxation in Fe-Doped $SrTiO_3$ systems: I. Single crystals, J. Am. Ceram. Soc. 91 (2008) 3245–3250.

[10] W. Liu, C.A. Randall, Thermally stimulated relaxation in Fe-Doped SrTiO3 Systems: II. Degradation of $SrTiO_3$ dielectrics, J. Am. Ceram. Soc. 91 (2008) 3251–3257.

[11] G.Y. Yang, G.D. Lian, E.C. Dickey, C.A. Randall, D.E. Barber, P. Pinceloup, M.A. Henderson, R.A. Hill, J.J. Beeson, D.J. Skamser, Oxygen nonstoichiometry and dielectric evolution of $BaTiO_3$. Part II - insulation resistance degradation under applied dc bias, J. Appl. Phys. 96 (2004) 7500–7508.

[12] T. Baiatu, R. Waser, K.H. Hardtl, Dc electrical degradation of perovskite-type titanates .3. A model of the mechanism, J. Am. Ceram. Soc. 73 (1990) 1663–1673.

[13] T. Holbling, N. Soylemezoglu, R. Waser, A mathematical-physical model for the charge transport in p-type $SrTiO_3$ ceramics under dc load: maxwell-Wagner relaxation, J. Electroceramics 9 (2002) 89–102.

[14] R. Meyer, R. Liedtke, R. Waser, Oxygen vacancy migration and time-dependent leakage current behavior of $Ba_{0.3}Sr_{0.7}TiO_3$ thin films, Appl. Phys. Lett. 86 (2005) 112904.

[15] Y. Cao, J. Shen, C. Randall, L.Q. Chen, Effect of ferroelectric polarization on ionic transport and resistance degradation in $BaTiO_3$ by Phase-field approach, J. Am. Ceram. Soc. 97 (2014) 3568–3575.

[16] D. Damjanovic, Ferroelectric, dielectric and piezoelectric properties of ferroelectric thin films and ceramics, Rep. Prog. Phys. 61 (1998) 1267–1324.

[17] D. Damjanovic, Stress and frequency dependence of the direct piezoelectric effect in ferroelectric ceramics, J. Appl. Phys. 82 (1997) 1788–1797.

[18] Y. Xiao, K. Bhattacharya, Interaction of oxygen vacancies with domain walls and its impact on fatigue in ferroelectric thin films, in: Smart Structures and Materials 2004: Active Materials: Behavior and Mechanics 5387, 2004, pp. 354–365.

[19] Y. Xiao, V.B. Shenoy, K. Bhattacharya, Depletion layers and domain walls in semiconducting ferroelectric thin films, Phys. Rev. Lett. 95 (2005) 247603.

[20] Q.S. Zhang, W.A. Goddard, Charge and polarization distributions at the 90 degrees domain wall in barium titanate ferroelectric, Appl. Phys. Lett. 89 (2006) 182903.

[21] J. Hlinka, P. Marton, Phenomenological model of a 90 degrees domain wall in $BaTiO_3$-type ferroelectrics, Phys. Rev. B 74 (2006) 104104.

[22] C. Korte, N. Schichtel, D. Hesse, J. Janek, Influence of interface structure on mass transport in phase boundaries between different ionic materials Experimental studies and formal considerations, Monatsh Chem. 140 (2009) 1069–1080.

[23] N. Schichtel, C. Korte, D. Hesse, J. Janek, Elastic strain at interfaces and its influence on ionic conductivity in nanoscaled solid electrolyte thin films-theoretical considerations and experimental studies, Phys. Chem. Chem. Phys. 11 (2009) 3043–3048.

[24] H.L. Hu, L.Q. Chen, Computer simulation of 90 degrees ferroelectric domain formation in two-dimensions, Mater. Sci. Eng. A Struct. Mater. Prop. Microstruct. Process. 238 (1997) 182–191.

[25] Y.L. Li, S.Y. Hu, Z.K. Liu, L.Q. Chen, Phase-field model of domain structures in ferroelectric thin films, Appl. Phys. Lett. 78 (2001) 3878–3880.

[26] Y.L. Li, S.Y. Hu, Z.K. Liu, L.Q. Chen, Effect of substrate constraint on the stability and evolution of ferroelectric domain structures in thin films, Acta Mater 50 (2002) 395–411.

[27] Y.L. Li, L.Q. Chen, G. Asayama, D.G. Schlom, M.A. Zurbuchen, S.K. Streiffer, Ferroelectric domain structures in $SrBi_2Nb_2O_9$ epitaxial thin films: electron microscopy and phase-field simulations, J. Appl. Phys. 95 (2004) 6332–6340.

[28] Y.L. Li, L.E. Cross, L.Q. Chen, A phenomenological thermodynamic potential for $BaTiO_3$ single crystals, J. Appl. Phys. 98 (2005) 064101.

[29] F.A. Kroger, H.J. Vink, Relations between the concentrations of imperfections in crystalline solids, Solid State Phys. 3 (1956) 307–435.

[30] L.Q. Chen, J. Shen, Applications of semi-implicit Fourier-spectral method to phase field equations, Comput. Phys. Commun. 108 (1998) 147–158.

[31] Y. Cao, S. Bhattacharya, J. Shen, C.A. Randall, L.Q. Chen, Role of polaron hopping in leakage current behavior of a $SrTiO_3$ single crystal, J. Appl. Phys. 114 (2013) 224102.